machines

MDPI

Article

Experimental Estimation of the Camber Reduction Factor of Tyres

Matteo Mottola and Matteo Massaro *

Department of Industrial Engineering, University of Padova, Via Venezia 1, 35131 Padova, Italy
* Correspondence: matteo.massaro@unipd.it

Abstract: One of the most used tyre models is the so-called Magic Formula, which provides the contact forces and moments as a function of the tyre slips and normal load. Among the slip inputs, there is the spin–slip, which is defined as the combination of a camber component and a path-curvature component. The two components are related to each other by the camber reduction factor, for which only a few data have been reported in the literature. In addition, these data are often obtained from indirect measurements. In this work, an experimental procedure for the direct measurement of the camber reduction factor was devised, and applied to six specimens of motorcycle tyres (three front and three rear). The approach employs a rotating-disk machine, where the tyre is intrinsically subjected to path curvature. A specific aligning procedure to mitigate sideslip disturbances is introduced and employed during testing. The three specimens of the rear tyres tested showed a camber reduction factor that was close to zero, which is the typical result suggested by the literature. On the contrary, the three specimens of front tyres showed slightly negative values, i.e., the camber component increased with respect to the curvature component. The results suggest that the classic assumption of a zero camber reduction factor does not hold valid for all motorcycle tyres.

Keywords: tyres; magic formula; camber; spin slip; turn slip

Citation: Mottola, M.; Massaro, M. Experimental Estimation of the Camber Reduction Factor of Tyres. *Machines* **2022**, *10*, 921. https://doi.org/10.3390/machines10100921

Academic Editor: Domenico Mundo

Received: 7 September 2022
Accepted: 5 October 2022
Published: 10 October 2022

1. Introduction

Several models have been developed over the years for the simulation of the response of tyres, including analytical/physical models such as the Brush models [1–4], semi-empirical models such as the so-called Magic Formula models [5–9] and complex finite-element models such as FTire and CDTyre [10,11].

The Magic Formula models are among the most used, and their inputs consist of the normal load and tyre slips, namely sideslip (or lateral slip), slip ratio (or longitudinal slip) and spin–slip. The latter is defined as the ratio between the component of the angular velocity normal to the road plane ω_z and the forward speed v [12]. Both the yaw rate $\dot{\psi}$ and spin Ω of the tyre contribute to ω_z. As a consequence, the spin–slip φ_s can be divided in two components

$$\varphi_s = -\frac{\omega_z}{v} = -\frac{\dot{\psi}}{v} + \frac{\Omega \sin\gamma}{v}, \tag{1}$$

where γ represents the camber angle. Theoretically, the same spin–slip can be equivalently generated using either the first term (called turn slip φ_t) or the second term (related to camber). However, it has been found that the effect of the two spin–slip components on the tyre response may not be the same. The practical solution is to introduce a camber reduction factor ε_γ in (1), obtaining [7]

$$\varphi_s = -\frac{\dot{\psi}}{v} + (1 - \varepsilon_\gamma)\frac{\Omega \sin\gamma}{v}. \tag{2}$$

When $\varepsilon_\gamma = 0$, the two components of the spin–slip are equivalent, whereas when $\varepsilon_\gamma = 1$, the camber has no effect on the spin–slip. The practical implication is that, when $\varepsilon_\gamma > 0$, the camber angle that is employed by the tyre-response model to generate spin–slip forces and

moments is attenuated. On the contrary, when $\varepsilon_\gamma < 0$, the camber angle that is employed by the tyre-response model to generate spin–slip forces and moments is amplified.

The reason for the camber reduction factor has been theorised by several explanations, both physical and analytical. In [12], it was associated with the flattening of a loaded tyre while cambered against a frictionless surface. In this case, the belt is distorted and the curvature of the peripheral line may reduce. As a consequence, the lateral distortion generated while rolling (in the cambered and loaded configuration) on a road is also reduced, hence the need for a camber reduction factor in the camber component of the spin–slip. The analogy between camber and spin is analytically supported in [13] in the case of small slips, i.e., large curvature radii. In [4,14] the two-dimensional field of velocity and stress that arises in the contact patch is analytically derived, supporting the idea that the two components of the spin–slip are related, although not exactly equivalent.

Regardless of the very nature of the reduction factor ε_γ, very few data have been reported in the literature for such factor. The relationship between turn slip and camber forces with different tyre carcass shapes, namely toroidal (motorcycles) and cylindrical (cars and trucks) was discussed in [12]. An experimental procedure for the determination of tyre response to turn slip and camber is presented. As the tyre tests carried out on a flat track, a direct measurement of turn slip response is not possible. Therefore, the transient response to a turn slip impulse, i.e., a yaw angle step, is used to derive the steady-state response to a turn slip step. The following procedure is employed: the tyre, with no camber neither sideslip, is lowered on the ground of the tyre test machine with a given negative yaw angle and is then loaded with the vertical force. Then, a positive yaw step is given in order to restore tyre yaw alignment. After the rolling motion starts, the tyre shows a transient lateral force response. By integration, the transient response to a turn slip step is derived from the measured data. Finally, the steady-state response to a turn slip step is the horizontal asymptote of the integration result. The results for a car tyre are shown, finding a camber reduction factor $\varepsilon_\gamma = 0.54$, which is obtained from the ratio between turn slip and camber forces. A slightly lower camber reduction factor $\varepsilon_\gamma = 0.43$ obtained from the moment response is also presented; however, the ε_γ obtained from forces is thought to be more representative, and the moment is less important.

The camber reduction factor that may be expected for a motorcycle tyre should be very different from that shown in [12] for a cylindrical tyre which, as when its belt curvature is distorted when cambered and loaded, it typically shows a reduced camber stiffness when compared against a toroidal tyre. According to [12], a camber reduction factor $\varepsilon_\gamma \approx 0$ is expected to represent the spin–slip behaviour of motorcycle tyres, however, no experimental results regarding motorcycle tyre camber reduction factor were found in the literature. On the MF-62 manual [7], which is one of the most used versions of the Magic Formula, some guidelines related to the camber reduction factors are given: on truck tyres, ε_γ may become slightly greater than 1, on car tyre ε_γ may reach values up to 0.7, while on motorcycle tyres, it is close to zero. Basically, the same guidelines are also suggested in [1].

The first contribution of this work is to devise an experimental method to directly measure the camber reduction factor of tyres on rotating-disk machines. The procedure is explained and the most relevant issues to reduce measurement errors are highlighted. The second contribution is the application of the method to six specimens of motorcycle tyres, which serves two purposes. The first is to demonstrate the practical application of the proposed method. The second purpose is to provide experimental evidence to the literature which is currently lacking such data for motorcycle tyres.

The paper is organised as follows. The test rig employed is described in Section 2, together with the methods for minimising tyre misalignments. Section 3 discusses the procedure for the experimental estimation of the camber reduction factor. Section 4 illustrates the findings, while Section 5 remarks some keypoints of the procedure involved.

2. Tyre Testing Machine

The properties of tyres under test are measured with the tyre test rig [15–17] of the University of Padova; Figure 1. This consists of a rotating disk with a diameter of approximately 3 m and a high-friction ring-like cover (sandpaper P120). The rotation, around the vertical axis, is driven by an electric motor. The free-rolling wheel is held in position with an articulated arm which, by means of two servomotors, allows to set the camber and sideslip angles. By means of three loadcells, the tyre lateral force, yaw moments and rolling resistance moment are acquired. The vertical load is set by adding weights to the structure.

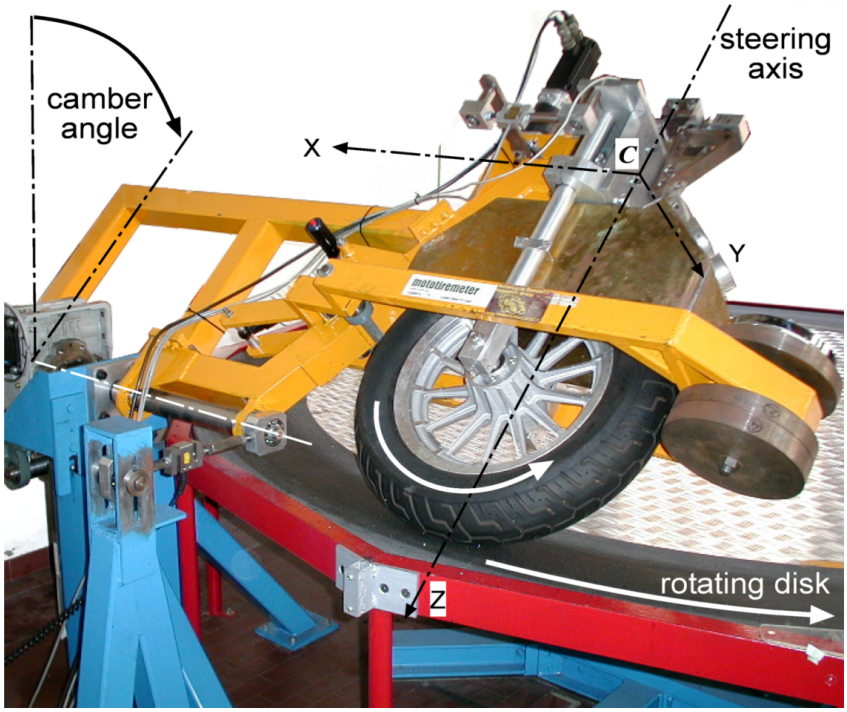

Figure 1. Tyre test rig layout. The tyre rolls freely on the rotating disk and is held in position by an articulated structure. The whole structure can camber with respect to the ground. The front assembly—which holds the wheel in place—can steer with respect to the cambered structure. Steel disks sets the vertical load.

Due to the path curvature, the tyre under test constantly exhibits a turn slip-related force that superimposes over camber-related and sideslip-related forces. This means that the raw generalised force measured by the machine $F_{raw}(\alpha, \gamma)$ at a given sideslip α and camber γ angles is the sum of the tyre response to those angles $F(\alpha, \gamma)$ and the tyre response to the turn slip $F(\varphi_t)$. During a standard measurement of tyre response to camber and sideslip angles, the turn slip force is therefore managed as a parasitic force that is identified and removed by means of a specific testing procedure. This is possible thanks to a symmetry assumption of tyre response. While the turn slip related force is always directed outwards from the disk centre, opposite camber and sideslip angles result in opposite forces

$$F(\alpha, \gamma) = -F(-\alpha, -\gamma). \tag{3}$$

Therefore, doubling the measurement of tyre response over symmetric angles, the response to camber and sideslip angles can be extracted through

$$F(\alpha, \gamma) = \frac{F_{raw}(\alpha, \gamma) - F_{raw}(-\alpha, -\gamma)}{2} \tag{4}$$

which leads to the decomposition of the measured response in its camber/sideslip and turn slip contributions.

While the path curvature of a rotating-disk test rig introduces these complications into the measurement procedure, when focusing on tyre turn slip behaviour, it is convenient because it allows to perform a direct measurement of turn slip force, simply measuring the tyre force response while rolling with no camber or sideslip angles:

$$F(\varphi_t) = F_{raw}(\alpha = 0, \gamma = 0) \tag{5}$$

2.1. Sideslip and Camber Response Measurements

The most standard tests performed on the machine are pure sideslip and pure camber tests, that are the measurements of the tyre's response to sideslip only $F(\alpha, \gamma = 0)$ or to camber only $F(\alpha = 0, \gamma)$, in terms of side force F_y and yaw moment M_z.

In practice, in a pure sideslip test (see e.g., Figure 2), the raw steady-state tyre response measurement $F_{raw}(\alpha)$ is repeated for a vector of sideslip angles $\boldsymbol{\alpha}$ and its opposite $-\boldsymbol{\alpha}$ while maintaining a camber angle equal to zero. Each point of the raw curve $F_{raw}(\alpha)$ is obtained by a time average of a large number of samples (typically, a 60 s $\div$ 120 s time window is involved, which corresponds to several tyre rotations and allows to exclude from the time averaging the transient part of the response). Finally, the tyre response curve to pure sideslip $F(\alpha)$ is obtained from the raw curve by removing the turn slip force through the application of (4). The same applies for a pure camber test, with the only difference of measuring the tyre's response $F(\gamma)$ to different camber angles $[\boldsymbol{\gamma}, -\boldsymbol{\gamma}]$ while maintaining a sideslip angle $\alpha = 0$ equal to zero.

A sideslip/camber coupled test could also be performed. In practice, the cross influence of the superimposition of these two quantities is analysed by observing the tyre response $F(\alpha, \gamma = \hat{\gamma})$ to sideslip at a fixed camber $\hat{\gamma}$. The test is similar to a pure sideslip test, i.e., measuring the tyre response over a sideslip angle vector $[\boldsymbol{\alpha}, -\boldsymbol{\alpha}]$, but at a given camber angle $\gamma = \hat{\gamma}$. However, for the turn slip component removal, in according to (4), for every measurement point $(\hat{\alpha}, \hat{\gamma})$, its opposite $(-\hat{\alpha}, -\hat{\gamma})$ is also needed. The measurement is therefore repeated, imposing an opposite camber angle $\gamma = -\hat{\gamma}$. Once the whole dataset $F_{raw}([\hat{\boldsymbol{\alpha}}, -\hat{\boldsymbol{\alpha}}], [\hat{\gamma}, -\hat{\gamma}])$ is obtained, with the application of (4), the desired tyre response curve $F(\alpha, \gamma = \hat{\gamma})$ is computed.

2.2. Alignment

A critical aspect regarding these measurement is tyre alignment, i.e., correctly setting the machine reference zero position for both axes α and γ. This is not a complex task when aligning the camber axis. The criterion is indeed the orthogonality between the wheel symmetry plane and rotating disk plane. The camber axis alignment is therefore straightforward. Furthermore, a fraction of degree as a residual misalignment would not be effective in compromising the measurements since it would be small if compared to the camber angles imposed during tests (up to 60 degrees for motorcycle tyres).

On the contrary, the sideslip axis is more demanding. The criterion is now the intersection between the wheel and rotating disk spin axes. This is a far more complex geometrical relation when compared to camber alignment and its practical realisation could lead to bigger errors. Furthermore, the tyre response in terms of F_y and M_z are very sensitive to sideslip angles and 0.5° misalignment in the slip axis would completely compromise the results. However, when using the geometry of the machine itself for the slip axis alignment, some tenths of a degree of error in the alignment process are in any case possible. For this purpose, a different alignment criterion is adopted, based on the tyre response. Instead of the input of the system (sideslip angle), the output (sideslip force) is used for the alignment since the system exhibits great gain between the input and output and the latter could be managed with smaller relative error.

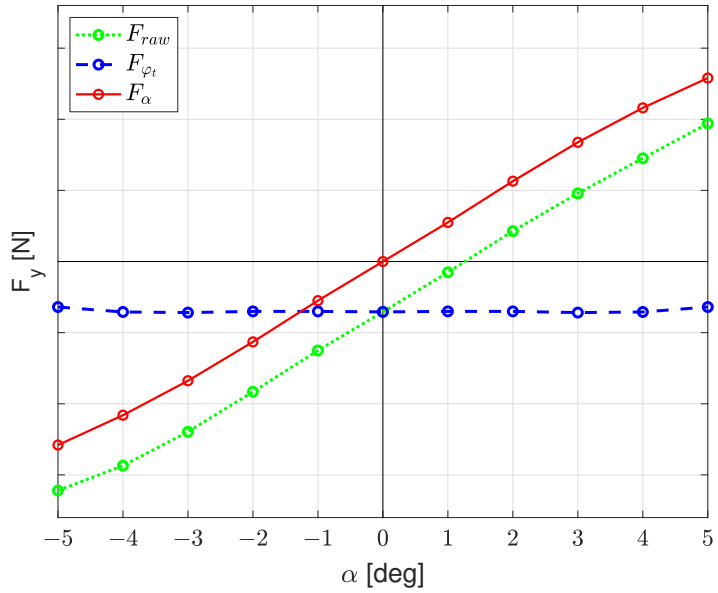

Figure 2. Example of a pure sideslip measurement. The dotted green curve is the raw tyre lateral force, the red solid line is the sideslip-related force obtained with the application of (4), while the blue dashed line is the turn slip force obtained as the difference between raw force and sideslip force. Note that, at zero sideslip, the dotted green and dashed blue curves coincide, as expressed by (5).

The criterion was called "forwards–backwards aligning technique" since it consists of the comparison of the raw tyre side force $F^F_{y,raw}$ that arises when free rolling in the standard (forward) direction versus the raw tyre force $F^R_{y,raw}$ that arises when free rolling backwards. The rolling direction change allows to uncover the sideslip-alignment status. Indeed, the turn slip force is always pointing outwards from the rotating disk, regardless of the rolling direction. Therefore, as the path curvature remains the same, the force magnitude also remains the same. On the contrary, the sideslip force changes its sign with the rolling direction. As a consequence, if there is a nonzero sideslip angle, the tyre exhibits a different side force when switching the rolling direction. Furthermore, these properties enable the extraction of the turn slip component as the mean of the two measurements

$$F_{y,\varphi_t} = \frac{F^F_{y,raw} + F^B_{y,raw}}{2}, \tag{6}$$

and the sideslip component as the deviation from the average

$$F_{y,\alpha} = F^F_{y,raw} - F_{y,\varphi_t}. \tag{7}$$

In other words, a tyre is assumed in a zero sideslip condition when the lateral force remains the same while rolling forwards or backwards. This behaviour leads to an iterative process that converges in the zeroing of the sideslip axis.

In practice, this process can be reduced to two iterations (i.e., two measurements of the lateral forces in forward and backward motion) as explained below. Firstly, the sideslip axis is geometrically aligned, with an estimated residual error of some tenth of a degree. Then, the first of the two measurements is performed, obtaining the lateral force $F^{F,(1)}_{y,raw}$ in forward motion and the lateral force $F^{B,(1)}_{y,raw}$ in the backward motion. The test rig steering axis is now rotated in order to correct the sideslip and reduce the sideslip lateral force. A root-solving

algorithm is therefore employed in order to calculate the requested rotation. In the first iteration, the sideslip offset is computed with a guess of the cornering stiffness using

$$\Delta\alpha^{(1)} = -\frac{F_{y,\alpha}^{(1)}}{C_\alpha^{(1)}}, \tag{8}$$

where $F_{y,\alpha}^{(1)}$ is the sideslip lateral force obtained with (7) from the first iteration measurements, $C_\alpha^{(1)}$ is the guess of the tyre cornering stiffness based on the tyre vertical load and on the typical normalised cornering stiffness of motorcycle tyres (a guess cornering stiffness per unit normal load of $C_\alpha^{(1)} = 10\,\mathrm{rad}^{-1}$ was employed in these tests), while $\Delta\alpha^{(1)}$ is the sideslip correction to be applied at the first iteration.

After the application of the $\Delta\alpha^{(1)}$ offset, the second iteration measurements $F_{y,raw}^{F,(2)}$ and $F_{y,raw}^{B,(2)}$ are taken and the second iteration sideslip force $F_{y,\alpha}^{(2)}$ is computed. The cornering stiffness guess is now corrected with the experimental data by using

$$C_\alpha^{(2)} = \frac{F_{y,\alpha}^{(2)} - F_{y,\alpha}^{(1)}}{\Delta\alpha^{(1)}} \tag{9}$$

The forwards–backwards aligning procedure ends with the application of the second iteration sideslip offset

$$\Delta\alpha^{(2)} = -\frac{F_{y,\alpha}^{(2)}}{C_\alpha^{(2)}}. \tag{10}$$

At this point, the tyre was considered aligned. Indeed, the curve $F_y(\alpha)$ is usually linear for small sideslip angles, and thus the process ideally provides the exact solution.

3. Method

In the case of a free rolling tyre with zero sideslip, the expression in (2) becomes

$$\varphi_s = -\frac{1}{R} + \frac{1-\varepsilon_\gamma}{r_e}\sin\gamma, \tag{11}$$

where R is the path-curvature radius of the tyre trajectory and r_e is the effective radius (also called rolling radius), where $\frac{\Omega}{v} = \frac{1}{r_e}$. In the case of small camber angles, (11) is further simplified to

$$\varphi_s \approx -\frac{1}{R} + \frac{1-\varepsilon_\gamma}{r_e}\gamma. \tag{12}$$

For small angles, the spin–slip force can thus be rewritten with the spin–slip stiffness C_{φ_s}

$$\begin{aligned} F_{y,\varphi_s} &= C_{\varphi_s}\varphi_s \\ &\overset{(12)}{=} C_{\varphi_s}\left(-\frac{1}{R} + \frac{1-\varepsilon_\gamma}{r_e}\gamma\right). \end{aligned} \tag{13}$$

when the tyre is subjected to turn slip only, the spin–slip force (13) can be rewritten as $F_{y,\varphi_s} = C_{\varphi_s}\varphi_t = C_{\varphi_t}\varphi_t$, with $\varphi_t = -\frac{1}{R}$, and therefore, the spin–slip stiffness coincides with the turn slip stiffness:

$$C_{\varphi_s} = C_{\varphi_t}. \tag{14}$$

when the tyre is subjected to camber only, the spin–slip force (13) can be rewritten as

$$\begin{aligned} F_{y,\varphi_s} &= C_{\varphi_s}\frac{1-\varepsilon_\gamma}{r_e}\gamma \\ &= C_\gamma\gamma. \end{aligned} \tag{15}$$

and therefore by substituting (14) into (15), the camber stiffness becomes

$$C_\gamma = C_{\varphi_t} \frac{1 - \varepsilon_\gamma}{r_e}. \tag{16}$$

Finally, making the camber reduction factor explicit, the following equation is obtained:

$$\varepsilon_\gamma = 1 - r_e \frac{C_\gamma^{F_y}}{C_{\varphi_t}^{F_y}}. \tag{17}$$

The camber reduction factor can therefore be determined by three measurements, namely the tyre effective radius r_e, the camber stiffness $C_\gamma^{F_y}$, and the turn slip stiffness $C_{\varphi_t}^{F_y}$. The methods involved in the derivation of these quantities are discussed below.

The tyre effective radius r_e is measured through the tyre angular displacement after its free rolling over a path of known length. The latter is chosen to be a full test rig disk rotation, which coincides with the circumference associated to the path curvature radius R. The measurement process begins by lowering to the ground and loading with vertical force the tyre with no sideslip or camber angles. Reference notches on disk, machine structure and tyre rim set the reference initial positions for the rolling test. The disk is then moved until a full circumference has been exploited by the tyre, and thus its rotation is stopped when the disk/machine reference notches match again. The tyre angular displacement $\Delta\vartheta = \vartheta_f - \vartheta_i$ that has been exploited during the test is traced counting the number of full revolutions and measuring the tyre's notch initial and final angular positions with an inclinometer. The ratio

$$r_e = \frac{\Delta L}{\Delta\vartheta} \tag{18}$$

provides the effective radius, where ΔL is the effective linear travel of the tyre. This quantity is not exactly equal to the circumference associated with the path curvature $C = 2\pi R$ since the initial and final rotating disk positions' misalignments may occur. The travelled distance then becomes $\Delta L = C_i + 2\pi R + C_f$ where C_i and C_f are, respectively, the initial and final misalignment of the disk's reference notches. These are nominally equal to zero $C_i = C_f = 0$. However, due to visual alignment, an uncertainty of approximately one millimetre is attributed to them: $u_{C_i}, u_{C_f} = \pm 1\,\text{mm}$. Similarly, the tyre angular measurements ϑ_f and ϑ_i are subjected to uncertainty of approximately one degree $u_{\vartheta_i}, u_{\vartheta_f} = \pm 1^\circ$

The nominal turning radius R of the tyre test rig is fixed and known, however for the current study, a precise measure is mandatory. The measured distance extends from the disk shaft axis to the tyre's contact patch centre, whose location is defined as the point equidistant from the left and right sidewalls. A concatenation of four single measures (shaft diameter, abrasive path diameter from shaft diameter, right sidewall from abrasive path diameter, and left sidewall from abrasive path diameter) are carried out in order to derive R. Following the measurement scheme in Figure 3, the path-curvature radius is obtained from

$$R = \frac{\Phi_A}{2} + L_B + \frac{L_C + L_D}{2}, \tag{19}$$

where each of the four arguments are defined in Figure 3 and are physically measured with an uncertainty of $u_i = \pm 1\,\text{mm}$.

The camber force stiffness computation is straightforward once a pure camber test is carried out. This value is computed as the slope of the force curve $F_{y,\gamma}(\gamma)$ around the camber is equal to zero $\gamma = 0$. Due to tyre symmetry assumption, the camber-stiffness is obtained from

$$C_\gamma^{F_y} = \frac{F_y(\hat{\gamma}_1)}{\hat{\gamma}_1}, \tag{20}$$

where $\hat{\gamma}_1 = 15^\circ$ is the angle used.

The turn slip-related side force F_{y,φ_t} is expressed in terms of turn slip $\varphi_t = -\dot{\psi}/v$ which, for a free-rolling tyre, becomes equal to the path curvature $\varphi_t = -1/R$. The turn slip force stiffness is the initial slope of the force curve. On a rotating-disk test rig, this quantity may be estimated as the ratio between the pure turn slip force and the path curvature. As already explained in (5), being a pure-turn slip condition coincident with the $\alpha = \gamma = 0$ condition, the turn slip force stiffness may be computed from

$$C_{\varphi_t}^{F_y} = \frac{F_{y,raw}([\alpha, \gamma] = 0)}{-1/R} = -F_{y,raw}([\alpha, \gamma] = 0)R, \tag{21}$$

where R is the path curvature. Again, a pure camber test is enough since the requested quantity coincides with the raw force measurement at $\gamma = 0$.

Note that the accuracy and precision in the F_{y,φ_t} measurement is critical to obtain an accurate and precise estimation of the camber reduction factor. This is evident when applying the error propagation formula [18]

$$u(y) = \sqrt{\sum_{i=1}^{I} \left[\left(\frac{\partial f}{\partial x_i} \right)_{x_i = \hat{x}_i} u_i(\hat{x}_i) \right]^2} \tag{22}$$

to (17) which relates the camber reduction factor to the test rig measurements. In fact, assuming typical values for the equation quantities ($R = 1.4\,\text{m}$, $C_\gamma^{F_y} = 2000\,\text{N/rad}$, $r_e = 0.3\,\text{m}$, $\varepsilon_\gamma = 0$), an uncertainty of approximately $u_{\varepsilon_\gamma} = \pm 0.1$ on the camber reduction factor is obtained with a uncertainty on the turn slip force of approximately only $F_{y,\varphi_t} = \pm 43\,\text{N}$.

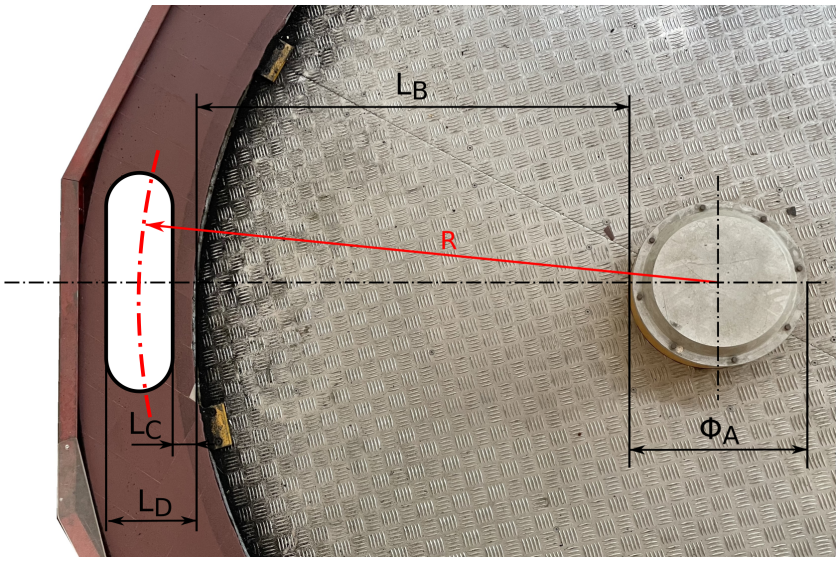

Figure 3. Top view of the tyre test rig. The path-curvature radius R is calculated through four measures, namely the rotating disk shaft diameter Φ_A, the radial distance of the ring-shaped annular path from disk's shaft L_B and the radial positions L_C and L_D of the inner and outer sidewall of the tyre, respectively.

For this reason, particular attention should be devoted to the measurement of F_{y,φ_t}, which may be affected by several disturbances. Firstly, F_{y,φ_t} is affected by camber and sideslip axes residual misalignments, as already discussed in Section 2. The camber misalignment is thought to be less than $\gamma_0 \leq 0.5°$ while the residual forwards–ackwards delta force is less than $\Delta F_y \leq 50\,\text{N}$.

Secondly, since the measure of the turn slip force is an absolute (note that every standard α and γ tyre response measurement consists of a relative force measurement)

force measurement, the loadcell offset value $F_{y,0}$ may also introduce uncertainties in the result. In fact, before every measurement, after the tyre is lowered to the ground and loaded with the vertical force (i.e., in a condition where no lateral deformations occur), a reset in the loadcells is performed. This is necessary in order to set the reference input value that corresponds to zero forces and moments to the acquisition system. However, if some unwanted lateral deformations are present on tyre tread during the loadcell reset process, a loadcell offset disturbance is introduced in the measurement chain. An investigation provides an estimated loadcell offset uncertainty of approximately $u_{F_{y,0}} = \pm 10\,\mathrm{N}$.

Another disturbance on F_{y,φ_t} is introduced by the sideslip axis actuation system. The sideslip axis servomotor is connected to the front assembly through a linkage in series to a planetary gearbox. Although the gearbox is of a reduced backlash type, at a M_z torque inversion, $\Delta\alpha_b$ follows. The tyre could therefore assume a sideslip angle that is different from zero and generates the related sideslip force. However, there is no possibility to identify this disturbance with a force measurement. The backlash disturbance is therefore analysed, measured and treated as a deterministic event in order to remove it in the aftermath from the measurement chain. Since the mechanism compliance makes the backlash a torque-dependent phenomenon, the measurement involves the application to the wheel of a torque of a typical magnitude ($M_z \approx 3\,\mathrm{Nm}$) that is generated by the wheel during free rolling on the rotating disk curved path. A centesimal comparator is used to measure the tangential displacement of the front assembly tangential displacement. The wheel backlash is finally estimated to be $\Delta\alpha_b = 0.17°$. Note that this quantity coincides with the sideslip angle variation when rolling forwards vs. backwards and does not compromise the forwards/backwards aligning procedure since it has the effect of equally reducing the F_y in both the rolling direction. After the alignment process, the tyre has a nominally zero sideslip angle. However, when rolling, the M_z torque makes the tyre assume a $\pm\Delta\alpha_b/2 = \pm 0.085°$ sideslip angle. In particular, when rolling forwards, the sign of the turn slip torque makes the tyre assume a $\alpha_b = -0.085°$ backlash-induced sideslip angle. Thanks to the availability of sideslip test measurements, the cornering stiffness is known and the backlash-induced parasite force is finally estimated as $F_{y,b} = C_\alpha^{F_y}\alpha_b$.

Finally, the turn slip force $F_{y,\varphi_t} = F_{y,raw}(\alpha = 0, \gamma = 0) - F_{y,b}$ is obtained with the removal of the backlash disturbance from the measured raw force. The residual uncertainties over this measurement are therefore related to the camber and sideslip angle alignment uncertainties and to loadcell offset uncertainty. The uncertainty behind the backlash force is not considered since its effect is small when compared to the others.

4. Results

The camber reduction factor is evaluated with the use of (17) and the measurement uncertainty is evaluated with the use of the error propagation Formula (22).

The raw measured lateral force $F_{y,raw}$ is the sum of different contributes, namely the turn slip force F_{y,φ_t}, the loadcell offset force $F_{y,0}$, the misalignment-related camber force $F_{y,\gamma_0} = C_\gamma^{F_y}\gamma_0$, the misalignment-related sideslip force F_{y,α_0} which is known in terms of force after the forwards–ackwards aligning procedure and the backlash-related force $F_{y,b} = C_\alpha^{F_y}\alpha_b$. The difference

$$F_{y,\varphi_t} = F_{y,raw} - F_{y,0} - C_\gamma^{F_y}\gamma_0 - F_{y,\alpha_0} - C_\alpha^{F_y}\alpha_b \tag{23}$$

allows to estimate the turn slip force, where the camber stiffness $C_\gamma^{F_y}$ and cornering stiffness $C_\alpha^{F_y}$ are known, respectively, from pure camber and pure sideslip measurements. Loadcell offset, camber misalignment angle and sideslip misalignment force are nominally zero $F_{y,0} = \gamma_0 = F_{y,\alpha_0} = 0$.

With the application of the error propagation formula to (23), the turn slip force uncertainty is estimated as

$$u_{F_{y,\varphi_t}} = \sqrt{u_{F_{y,0}}^2 + \left(C_\gamma^{F_y} u_{\gamma_0}\right)^2 + u_{F_{y,\alpha_0}}^2 + \left(C_\alpha^{F_y} u_{\alpha_b}\right)^2} \tag{24}$$

where $u_{F_{y,0}} = \pm 10\,\mathrm{N}$ is the typical loadcell offset uncertainty, $u_{\gamma_0} = \pm 0.5^\circ$ is the typical camber angle misalignment uncertainty, $u_{F_{y,\alpha_0}} = \pm 25\,\mathrm{N}$ is the typical sideslip force misalignment uncertainty (since the typical residual misalignment forwards–backwards aligning procedure explained in Section 2 is $\Delta F_y < 50\,\mathrm{N}$ when switching rolling direction, the residual misalignment-related sideslip force during standard force measurements is $\Delta F_y/2$). As explained previously, the backlash angle uncertainty is zero as the term $C_\alpha^{F_y} u_{\alpha_b}$ is small when compared to other sources of uncertainty. The estimation of the turn slip force and its related uncertainty for the six tyres under test is shown exposed in Table 1.

Table 1. Turn slip force estimation. Note that the force values are reported as absolute values: the tyre testing machine curvature direction generates negative turn slip forces.

Tyre Code	F_{y,φ_t} (N)	$u_{F_{y,\varphi_t}}$ (N)
Front $n^\circ 1$	385.7	± 31.4
Front $n^\circ 2$	373.5	± 31.6
Front $n^\circ 3$	340.6	± 31.2
Rear $n^\circ 1$	493.7	± 32.2
Rear $n^\circ 2$	454.8	± 31.7
Rear $n^\circ 3$	488.5	± 32.1

The path curvature estimation provides a turning radius of $R = 1323\,\mathrm{mm}$ with a measurement uncertainty of approximately $u_R = \pm 1.8\,\mathrm{mm}$.

The final estimation of the camber reduction factor is obtained with the substitution into (17) of a list of indirect measurements. First, the rolling radius computation Equation (18) also requires the information of the turning radius R. Secondly, the camber side force stiffness estimated from pure camber measurements with the ratio of (20). Finally, the turn slip stiffness, estimated as in (21) with the product between turn slip force and turning radius R. Note that, as already discussed, in order to improve the accuracy and precision of the result, the force as estimated in Table 1 is used instead of the direct $F_{y,raw}([\alpha, \gamma] = 0)$ measurement.

The measurement error propagation on the computation of (17) is applied as with (22). The results are summarised in Table 2 and Figure 4. The three front tyres are all 120/70-17, however, they are different in construction. Similarly, the rear tyres are all 190/55-17, with different specifications from one another. The camber reduction factor values obtained for the rear tyres (last three rows) are in a band across $\varepsilon_\gamma = 0$ and are thus in agreement with the literature, which indeed suggests that motorcycle tyres should have a factor of almost zero. One the contrary, front tyres (first three rows of Table 2) exhibit different values of camber reduction factor, whose band extends towards negative values. The lowest obtained value is $\varepsilon_\gamma = -0.19$ and its confidence band is $u_{\varepsilon_\gamma} = \pm 0.11$. The confidence band is narrow enough to confirm the nonzero camber reduction factor. A negative factor means an amplification of the camber component over the turn slip component. In this specific case, the amplification is up to 20%.

Table 2. Camber reduction factor estimation.

Tyre Code	$\varepsilon_\gamma\,(-)$	$u_{\varepsilon_\gamma}\,(-)$
Front $n°1$	-0.0609	± 0.0863
Front $n°2$	-0.1245	± 0.0951
Front $n°3$	-0.1870	± 0.1089
Rear $n°1$	0.0174	± 0.0642
Rear $n°2$	-0.0064	± 0.0702
Rear $n°3$	0.0178	± 0.0646

It is worth stressing that these results are not to claim that all rear motorcycle tyres are with a zero camber reduction factor, and all front motorcycle tyres are with a negative factor. However, the experimental evidence suggests that the classic assumption of a zero camber reduction factor does not apply to all motorcycle tyres.

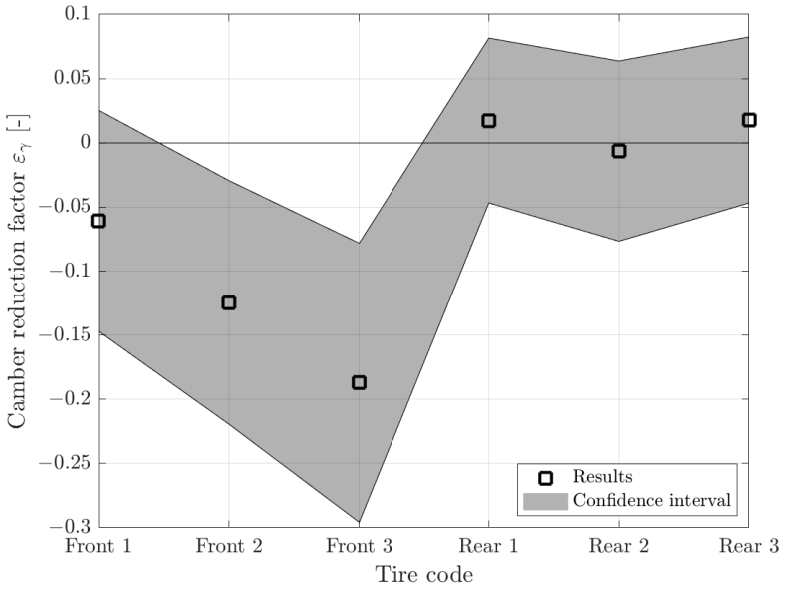

Figure 4. Camber reduction factor for the tested tyres.

5. Remarks

The importance of the forwards–backwards aligning procedure is discussed herein. If a sideslip misalignment α_M occurs, the forces and moments measured by the test rig at a nominal sideslip α_N are instead generated by a tyre operating at $\alpha = \alpha_N + \alpha_M$. The general effect on the obtained curve $F_{raw}(\alpha_N)$ is therefore a translation over the abscissa axis by a quantity equal to the misalignment α_M. When a similar misalignment occurs in a straight-path tyre testing machine, the sideslip offset can be easily handled. For example, in a MF-6.2 fitting perspective, the offset would not compromise the result and would be taken into account by the shift coefficients (PHY1, PHY2 [7]). However, in a rotating-disk test rig, due to the necessity of a symmetry hypothesis in order to remove the turn slip component as exposed in Section 2, a misalignment α_M is not allowed in the raw experimental curve.

In Figure 5, the effect of a misalignment $\alpha_M = -1°$ is shown. The measured curve $F_{raw}(\alpha)$ (green-dotted-starred line), i.e., the curve with the misalignment, is translated rightward (i.e., towards the positive direction of the sideslip axis) with respect to the real tyre characteristics $F_{raw}(\alpha_N)$ (green dotted-circled line). The tyre sideslip characteristics (red curves) are obtained with the application of (4) to the raw curve, while the turn slip characteristics are obtained through the difference between the raw curve and the sideslip curve

$$F_{\varphi_t}(\alpha) = F_{raw}(\alpha) - F_\alpha(\alpha). \tag{25}$$

The difference between the circled and starred turn slip force (blue) and sideslip force (red) curves reveals the effect of the misalignment.

Firstly, the turn slip force, when evaluated as in (5), is quite far from the actual value. In this example, a $F_{\varphi_t} = -671\,\mathrm{N}$ is measured, instead of a real turn slip force $F_{\varphi_t} = -300\,\mathrm{N}$. Secondly, the turn slip force curve obtained with the misalignment does not assume constant values, which is the expected behaviour, as the path curvature is constant during the test. Thirdly, the sideslip force curve is scaled. The misaligned curve (starred) shows smaller absolute values, and the cornering stiffness value (numerical derivative of the curve around $\alpha = 0$) decreases by 5%.

The effect of the misalignment in the camber reduction factor estimation is now discussed. The case study is a tyre with a rolling radius $r_e = 0.3\,\mathrm{m}$ that shows the curves in Figure 5 and is characterised by a camber reduction factor $\varepsilon_\gamma = 0$ when computed with the correct turn slip force (i.e., without any misalignments), that is $F_{\varphi_t} = -300\,\mathrm{N}$. If a slip axis misalignment of $\alpha_M = -1^\circ$ occurs in the experimental tests, the estimated camber-reduction factor would be approximately $\varepsilon_\gamma = 0.53$. A misalignment $\alpha_M = 1^\circ$ in the opposite direction would be an even worse scenario because, giving a positive turn slip force of about $F_{\varphi_t} = 71\,\mathrm{N}$, the resulting camber reduction factor would be approximately $\varepsilon_\gamma = 9.12$. When a misalignment of approximately $\alpha_M = -0.5^\circ$ occurs, which is a realistic situation when not applying the forwards–backwards aligning procedure and aligning the slip axis only with a geometrically-based approach, a camber reduction factor of approximately $\varepsilon_\gamma = 0.36$ would result from the computation, while the opposite misalignment $\alpha_M = 0.5^\circ$ would result in a camber reduction factor of approximately $\varepsilon_\gamma = -1.31$. The two examples discussed highlight the importance of a fine slip axis alignment procedure in order to properly estimate the camber reduction factor.

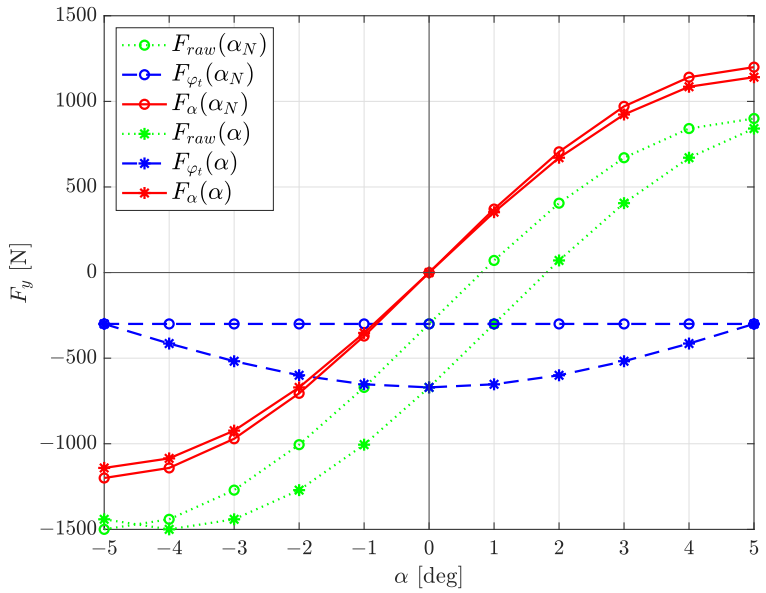

Figure 5. Effect of slip axis misalignment. Circled lines identify the tyre characteristics, and starred lines identify the same characteristics obtained with a misalignment.

6. Conclusions

The camber reduction factor of a motorcycle tyre, usually assumed to be approximately zero in the literature, was experimentally investigated and measured in this work. The rotating-disk tyre test rig employed was described, together with the methods and procedures used to experimentally extract the tyre characteristics. The measurement and derivation of each parameter belonging to the camber reduction factor equation were discussed, and the sources of disturbances and uncertainty were evaluated. The results of the study include an experimental procedure for the direct assessment of the camber reduction

factors, together with the values and confidence band of six specimens of motorcycle tyres. The experimental tests were carried out for two main reasons. The first was to demonstrate a practical application of the proposed procedure. The second was to provide experimental data related to motorcycle tyres, which are rarely considered in the literature. Nevertheless, the method is equally applicable to car tyres. The values of the camber reduction factor obtained are close to zero for the three rear tyres under test, as suggested by the literature. However, the same parameter assumes negative values for the three front tyres under test, where the farthest value stands at $\varepsilon_\gamma \approx -0.2$. The uncertainty band around this result is narrow enough to confirm that, for these tyres, the camber reduction factor is nonzero. This means that the contribution of the camber component may increase with respect to that of the curvature component in some motorcycle tyres, and that the camber reduction factor is not necessarily zero, as is often assumed.

Author Contributions: Conceptualisation, M.M. (Matteo Mottola) and M.M. (Matteo Massaro); methodology, M.M. (Matteo Mottola) and M.M. (Matteo Massaro); software, M.M. (Matteo Mottola); validation, M.M. (Matteo Mottola) and M.M. (Matteo Massaro); formal analysis, M.M. (Matteo Mottola); investigation, M.M. (Matteo Mottola) and M.M. (Matteo Massaro); writing—original draft preparation, M.M. (Matteo Mottola); writing—review and editing, M.M. (Matteo Mottola) and M.M. (Matteo Massaro); visualisation, M.M. (Matteo Mottola); supervision, M.M. (Matteo Massaro). All authors have read and agreed to the published version of the manuscript.

Funding: This research received no external funding.

Institutional Review Board Statement: Not applicable.

Informed Consent Statement: Not applicable.

Data Availability Statement: Not applicable.

Conflicts of Interest: The authors declare no conflict of interest.

References

1. Pacejka, H.B. *Tire and Vehicle Dynamics*, 3rd ed.; Butterworth Heinemann: Oxford, UK, 2012. [CrossRef]
2. Limebeer, D.; Massaro, M. *Dynamics and Optimal Control of Road Vehicles*; Oxford University Press: Oxford, UK, 2018. [CrossRef]
3. Guiggiani, M. *The Science of Vehicle Dynamics*; Springer: Dordrecht, The Netherlands, 2014. [CrossRef]
4. Romano, L.; Bruzelius, F.; Jacobson, B. Brush tyre models for large camber angles and steering speeds. *Veh. Syst. Dyn.* **2022**, *60*, 1341–1392. [CrossRef]
5. Bakker, E.; Nyborg, L.; Pacejka, H.B. Tyre Modelling for Use in Vehicle Dynamics Studies. *SAE Trans.* **1987**, *96*, 190–204. [CrossRef]
6. Besselink, I.J.; Schmeitz, A.J.; Pacejka, H.B. An improved Magic Formula/Swift tyre model that can handle inflation pressure changes. *Veh. Syst. Dyn.* **2010**, *48*, 337–352. [CrossRef]
7. TNO. *MF-Tyre/MF-Swift 6.2 Equation Manual*; TNO: Aja, The Netherlands, 2013.
8. Farroni, F.; Lamberti, R.; Mancinelli, N.; Timpone, F. TRIP-ID: A tool for a smart and interactive identification of Magic Formula tyre model parameters from experimental data acquired on track or test rig. *Mech. Syst. Signal Process.* **2018**, *102*, 1–22. [CrossRef]
9. Sakhnevych, A. Multiphysical MF-based tyre modelling and parametrisation for vehicle setup and control strategies optimisation. *Veh. Syst. Dyn.* **2021**, 1–22. [CrossRef]
10. Gipser, M. FTire—The tire simulation model for all applications related to vehicle dynamics. *Veh. Syst. Dyn.* **2007**, *45*, 139–151. [CrossRef]
11. Gallrein, A.; Bäcker, M. CDTire: A tire model for comfort and durability applications. *Veh. Syst. Dyn.* **2007**, *45*, 69–77. [CrossRef]
12. Pacejka, H.B. Spin: Camber and turning. *Veh. Syst. Dyn.* **2005**, *43*, 3–17. [CrossRef]
13. Higughi, A. Transient Response of Tyres at Large Wheel Slip and Camber. Ph.D. Thesis, Delft University of Technology, Delft, The Netherlands, 1997.
14. Romano, L.; Timpone, F.; Bruzelius, F.; Jacobson, B. Analytical results in transient brush tyre models: Theory for large camber angles and classic solutions with limited friction. *Meccanica* **2022**, *57*, 165–191. [CrossRef]
15. Cossalter, V.; Doria, A.; Lot, R.; Ruffo, N.; Salvador, M. Dynamic Properties of Motorcycle and Scooter Tires: Measurement and Comparison. *Veh. Syst. Dyn.* **2003**, *39*, 329–352. [CrossRef]
16. Massaro, M.; Cossalter, V.; Cusimano, G. The effect of the inflation pressure on the tyre properties and the motorcycle stability. *Proc. Inst. Mech. Eng. Part D J. Automob. Eng.* **2013**, *227*, 1480–1488. [CrossRef]
17. Cossalter, V.; Doria, A.; Giolo, E.; Taraborrelli, L.; Massaro, M. Identification of the characteristics of motorcycle and scooter tyres in the presence of large variations in inflation pressure. *Veh. Syst. Dyn.* **2014**, *52*, 1333–1354. [CrossRef]
18. Kline, S.; Mcclintock, F.M. Describing Uncertainties in Single-Sample Experiments. *Mech. Eng.* **1953**, *75*, 3–8.